Functionalization of graphene oxide sheets with magnetite nanoparticles for the adsorption of copper ions and investigation of its potential catalytic activity toward the homocoupling of alkynes under green conditions

Laroussi Chaabane, Emmanuel Beyou, Dominique Luneau, Mohammed Hassen V. Baouab

Functionalization of graphene oxide sheets with magnetite nanoparticles for the adsorption of copper ions and investigation of its potential catalytic activity toward the homocoupling of alkynes under green conditions

Laroussi Chaabane[a,b], Emmanuel Beyou[a,b,*] Dominique Luneau[c], Mohammed Hassen V Baouab[d]

[a]Ingénierie des Matériaux Polymères (IMP), Villeurbanne, F-69622, France.

[b]CNRS, UMR5223, Villeurbanne, F69621, Université de Lyon, F-69003, Lyon, France.

[c]Laboratoire des Multi matériaux et Interfaces, UMR CNRS 5615, Université de Lyon1, Université Lyon1, Villeurbanne F-69622, France

[d]Unité de Recherche Matériaux et Synthèse Organique (UR17ES31) Institut Préparatoire aux Etudes d'Ingénieurs de Monastir, Université de Monastir, Bd. de l'environnement, 5019 Monastir, Tunisie.

E-mail: beyou@univ-lyon1.fr

Abstract

This paper deals with the preparation of graphene oxide sheets (GO) modified with magnetite nanoparticles (Fe_3O_4NPs) for removing Cu(II) ions from aqueous solutions. Moroever, the recovered Cu(II)-based material was recycled as a catalyst for the homocoupling of a series of alkynes. The adsorption behavior of magnetic GO-based materials towards Cu(II) ions from aqueous solutions was studied as a function of the pH value and the contact time and it was observed that the magnetic GO-based absorbent can be separated quickly from its aqueous solution by using an external magnetic field. Its equilibrium adsorption capacity value for Cu(II) ions was as high as 3.808±0.125 $mmol.g^{-1}$ under neutral conditions. In addition, the catalytic activity of the resulting [GO-EDA-CAC@Fe_3O_4NPs]-BPED-Cu(II) material toward the homocoupling of phenylacetylene into 1,4-diphenylbuta-1,3-diyne was demonstrated with a yield up to 99%. Importantly, the [GO-EDA-CAC@Fe_3O_4NPs]-BPED-Cu(II) supported catalyst was consecutively reused for fifteen runs without a significant loss of its activity.

Keywords: Graphene oxide sheets; Removal of Cu(II) ions; Catalytic activity; Homo-coupling of alkynes; Green Conditions.

1. Introduction

With the rapid growth of industrial activities, water contamination by heavy metals ions has enhanced undesirable effects on both human health and environment considering their extreme toxicity, persistence, non-biodegradability, and bioaccumulation in the food chain [1-3]. One of the most diffuse toxic metal ions are copper ions (Cu (II)) coming from several industries including battery manufacturing, fertilizer industry, mining, and electroplating [4-7]. Nowadays, various methods and processes such as flocculation, ultrafiltration, electro-dialysis, reverse osmosis, and adsorption have been used to remove toxic metal ions from wastewater and water [8-11]. However, most of these methods require high operating costs and produce toxic sludge while the use of absorbents do not allow an easy recovering [12, 13]. Moreover, traditional adsorbents such as active carbon, biomass materials, and polymer resins suffer from poor adsorption sites and consequently display a low adsorption capacity [14-16]. Recently, various novel adsorbents based on functionalized carbon nanotubes and graphene oxide (GO) sheets have been developed [17].

In particular, GO displays a good adsorption capacity towards heavy metal ions due to the presence of epoxy, carboxyl, and hydroxyl functional groups onto their surface [18-22] and its functionalization can improve it [9, 23]. One of the attractive ways for modifying GO is the use of multifunctional organic molecules containing strong chelating groups [24, 25]. For instance, Laroussi *et al.*, [25] modified GO with *N,N*-bis(2-pyridylmethyl)ethylenediamine (BPED) for removing Cu(II), Ni(II) and Co(II) ions from aqueous solutions. However, the the obtained GO-based materials, having high dispersibility in aqueous solutions, did not permit to revover it easily. In this context, a few authors [26-28] studied the modification of GO with magnetic nanoparticles which allow its recovering by using an external magnetic field. Indeed, it is well known that magnetite nanoparticles (Fe_3O_4NPs) can be combined with GO sheets by various methods such as co-precipitation, solvothermal, and ionothermal [29].

The co-precipitation method is the most used technique to synthesize Fe_3O_4NPs because of its eco-friendly procedure [30]. For instance, Liu *et al.,* [31] prepared a magnetic-GO modified 1,2-diamineocyclohexanetetraacetic acid composite (GO-Fe_3O_4NPs-DCTA) and they studied the effect of multi-functional organic acid ligands on the adsorption of Cu(II) ions. The incorporation of metal ions onto magnetic GO-based materials provided a new strategy for the fabrication of atomic level-distributed metal catalysts.

In addition, the recyclability of GO-based absorbents containing metal ions is of great interest in particular for the catalysis of some organic reactions such as the homocoupling of alkynes. Indeed, homocoupling of alkynes is one of the conventional methods for the synthesis of symmetric 1,3-diynes [32]. This reaction is usually carried out in presence of copper salts, as catalyst [33]. For example, Wang *et al.,* [34] studied the homocoupling of terminal alkynes in the presence of $CuCl_2$ and Et_3N as the base under solvent-free conditions. Moreover, Singh *et al.,* [35] reported the homocoupling of terminal alkynes to symmetric 1,3-diynes using CuI, benzotraizole as the metal ligand and K_2CO_3 as the base in dimethylformamide (DMF). However, the heterogeneous catalysis is often preferred with regard to facile catalyst separation and recycling [36]. Recently, several copper-based heterogeneous catalytic systems for the oxidative homocoupling of terminal alkynes have been reported, such as CuI immobilized on 3-(2-aminoethylamino)propyl-functionalized (MCM-41) [37] and copper(I)-modified zeolites [38]. However, these catalytic systems require the use of high reaction temperatures and stabilizing ligands while displaying a low selectivity [39].

In the present study, we have designed a novel multi-functional magnetic GO-based adsorbent for high-efficiency removal of Cu(II) ions from aqueous solutions and having a catalytic activity toward the homocoupling of terminal alkynes. First, the magnetite nanoparticles (Fe_3O_4NPs) were successfully adsorbed onto GO sheets through a co-

precipitation method after the grafting of ethylenediamine (EDA) and chloroacetyl chloride (CAC) onto the GO sheets through an experimental procedure described in a previous work [25]. Then, the grafting of *N,N*-bis(2-pyridylmethyl)ethylenediamine (BPED) onto (GO-EDA-CAC)@Fe_3O_4NPs was characterized by FTIR, XPS, TGA, SEM, EDX, XRD, and VSM and the corresponding GO-based absorbent was used as an adsorbent to remove Cu(II) ions from aqueous solutions. The influence of the pH and contact time onto the Cu(II) ions adsorption capacities of the adsorbents were investigated, thoroughly. Finally, the resulting [GO-EDA-CAC@Fe_3O_4NPs]-BPED-Cu(II) material was reused as a catalyst for the homocoupling of a series of terminal alkynes under green experimental conditions.

2. Experimental

2.1. Reagents

Graphite powder was kindly provided by TIMCAL Graphite & Carbon, France (4 mm in size). Graphite Oxide (GO) was prepared using a modified Hummers' method by oxidation of natural graphite powder (4 µm in size, 99.99% purity) [25]. Ethylenediamine (EDA), chloroacetyl chloride, sodium carbonate (Na_2CO_3), sodium hydroxide (NaOH), nitric acid (HNO_3), *n*-butylamine, diisopropylamine, diethylamine, calcium carbonate ($CaCO_3$), tripotassium phosphate trihydrate ($K_3PO_4.3H_2O$), ferric chloride ($FeCl_3.6H_2O$) 98%, ferrous chloride tetrahydrate ($FeCl_2.4H_2O$) 99%, copper (II) chloride dihydrate ($CuCl_2.2H_2O$) 99%, sodium chloride, copper (I) bromide 99%, copper (I) chloride 99% and potassium hydrogen phthalate were purchased from Aldrich. Solvents such as dimethylformamide (DMF), dimethyl sulfoxide (DMSO), 1,4 dioxane, chloroform, tetrahydrofuran (THF), *n*-propanol, benzene, glycerol, *n*-hexane, ethyl acetate (EtOAc), methanol, ethanol, diethyl ether, ammonium hydroxide (NH_4OH) and all the substrates required for homocoupling were purchased from Aldrich and used as received. All aqueous solutions were diluted with deionized water (EC<0.05µs.m^{-1} ; Millipore system).

2.2. Instruments

Fourier transform-infrared spectroscopy (FTIR) were recorded using a Nicolet 460 spectrometer (Thermo Nicolet Corporation, USA) and samples in KBr pellet form. Thermogravimetric analysis (TGA) was investigated by Perkin Elmer thermal analyzer instrument (Nicolet, TA SDT Q600, USA) with a heating rate of 5 °C.min^{-1} and nitrogen gas flow at 50 mL min^{-1}. Powder X-ray Diffraction (PXRD) measurements were collected on a Siemens D500 diffractometer (Ni-filtered Cu, KR radiation, 1.5405 Å, FEI, USA). X-ray photoelectron spectroscopy (XPS) analysis were carried out on a Perkin Elmer PHI5300 physical spectrometer (SXM instrument, USA) with binding energy in the range -2 to 1400 eV. Scanning electron microscope (SEM) images were taken by a commercial FEI Company, Netherlands. Magnetic measurements were performed at 300 K on powdered samples packed in polycarbonate capsules using a Quantum Design MPMS-XL SQUID magnetometer. NMR spectra were recorded on a Brucker AC-600, USA spectrometer at 600 MHz (^{1}H) and 150 MHz (^{13}C). All chemical shifts were reported as δ values (ppm) relative to the residual non-deuterated solvent. EI-MS was determined with an Agilent 5975N mass spectrometer. The concentration of Cu(II) ions solutions were measured using an Uv-Visible Perkin Elmer, USA spectrophotometer through the formation of Cu(II) hydrogen phthalate complex.

2.3. Preparation of the GO-EDA-CAC)@Fe_3O_4NPs material

First, the GO-EDA-CAC substrate was prepared according to our previous work [25]. Then, 1.50 g of $FeCl_3.6H_2O$ and 0.75 g of $FeCl_2.4H_2O$ were added to a GO-EDA-CAC dispersion in 10 mL of deionized water followed by a sonication at 60 °C for 1 h. Subsequently, the pH of the corresponding aqueous suspension was adjusted to 10-11 by dropping 5.46 g of NH_4OH [29]. At the end of the reaction, the (GO-EDA-CAC)@Fe_3O_4NPs material was separated from the aqueous solution with the help of a magnet and washed

repeatedly with deionized water and ethanol and finally dried under vacuum at 80 °C overnight.

2.4. Grafting of BPED onto the GO-EDA-CAC@Fe_3O_4NPs substrate

According to the literature [25, 40], the preparation of *N,N*-bis(2-pyridylmethyl)-ethylenediamine (BPED) can be achieved using the synthetic route presented in Scheme 1 **(Section 1, Supporting information** †). So, 1 g of GO-EDA-CAC@Fe_3O_4NPs was dispersed in 40 mL anhydrous DMF and sonicated for 30 min. Then, 3.63 g of BPED and 3.95g of Et_3N were added in the suspension and stirred at 80 °C for 24 h. At the end of the reaction, the suspension was centrifugated and washed with ethanol to remove the free BPED molecules. The latter purification step was monitored by UV-Visible analysis. **(Fig. S1†).** Finally, the powder was dried under vacuum at 80 °C overnight.

2.5. Cu(II) adsorption experiments

The adsorption behavior of the two magnetic adsorbents (GO-EDA-CAC)@Fe_3O_4NPs and [(GO-EDA-CAC)@Fe_3O_4NPs]-BPED towards Cu(II) ions were studied in details. Thus, the effect of some operating parameters such as the pH and the contact time on the Cu(II) adsorption capcities were evaluated. First, the point of zero charge (pH_{pzc}) defined as the point where the density of the adsorbent electrical surface charge of adsorbent is zero **(section 2, Supporting information†)**. First, the effect of the pH on Cu(II) ions adsorption was studied in the range 3-8 and adjusted with a Clark-Lub's buffer solutions (0.1M HNO_3 and 0.1M NaOH) [41]. Experiments were performed by mixing 100 mg of the adsorbent into 100 mL of the Cu(II) ions aqueous solutions with $[C_0]$= 250 $mg.L^{-1}$. Then, the suspensions were sealed and stirred for 24 h at room temperature. When adsorption equilibrium was reached, the mixture was centrifuged at 5000 rpm for 10 min. In the case of the presence of a precipitate of $Cu(OH)_2$ in the aqueous solution at pH>7, the suspension was filtered through a 0.45 µm membrane filter. The initial and equilibrium concentrations of Cu(II) ions in the aqueous

solution were determined by UV-Vis spectrometry using calibration curves **(Table S1† and Fig. S2†)**.

The equilibrium adsorption capacity (Qe; mmol.g^{-1}) of the adsorbent was calculated with the following equation (Eq. 1) [42, 43]:

$$Q_e = \frac{V(C_0 - C_e)}{m} \quad (1)$$

Where C_0 and C_e are the initial and equilibrium concentrations (mmol.L^{-1}) of the Cu(II) ions aqueous solutions, respectively. V is the volume of the Cu(II) ions solution (mL) and m (mg) is the mass of the adsorbent.

2.6. Homocoupling of alkynes in presence of the [GO-EDA-CAC@Fe3O4NPs]-BPED-Cu(II) material

In a typical reaction, the terminal alkyne (1.00 mmol) and Na_2CO_3 (1.20 mmol) were dissolved in 2 mL of glycerol. Then, the supported copper catalyst [GO-EDA-CAC@Fe_3O_4NPs]-BPED-Cu(II) catalyst (10 mg) was added in the mixture and stirred at 80 °C for 30 min to 320 min. The reaction was monitored by TLC using EtOAc and *n*-hexane (1:4) as eluent and gas chromatography. After completion of the reaction, the reaction mixture was cooled to room temperature and diluted with water (5 mL), followed by the separation of the magnetic supported copper catalyst from the reaction mixture by using an external magnet. Then, the [GO-EDA-CAC@Fe_3O_4NPs]-BPED-Cu(II) catalyst was washed with methanol and dried carefully before use in the next run. The remaining products in the supernatant mixture was extracted with EtOAc (4×5 mL) and finally purified by column chromatography.

3. Results and discussion

As described in our previous article [25], GO-EDA-CAC was easily synthesized in two steps from GO sheets. However, the synthetic procedure involves a complementary step

based on the doping of GO-EDA-CAC with magnetite nanoparticles (Fe_3O_4NPs) through the co-precipitation method (scheme 1). Indeed, it is expected that the presence of Fe_3O_4NPs onto the GO-based surface will facilitate its recovering after the Cu(II) adsorption. Finally, the grafting of *N,N*-bis(2-pyridylmethyl)ethylenediamine groups (BPED) onto GO-EDA-CAC@Fe_3O_4NPs was realized in order to ensure higher Cu(II) ions adsorption **(Scheme 1)**.

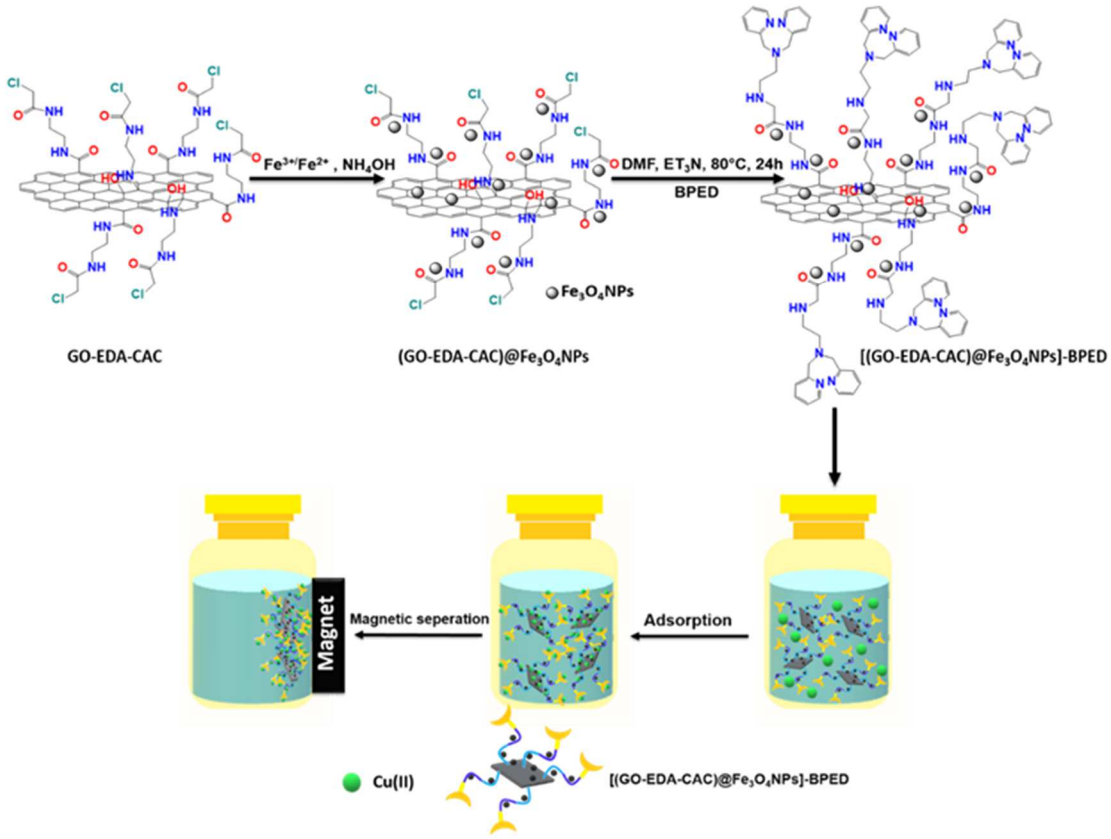

Scheme 1. Preparation of the GO-EDA-CAC@Fe_3O_4NPs-BPED absorbent followed by the adsorption of Cu(II) from aqueous solutions.

3.1. Synthesis and characterization of the GO-EDA-CAC@Fe3O4NPs-BPED absorbent

3.1.1. Doping GO-based materials with magnetite nanoparticles

As discussed before, the synthesis and the characterization of GO-EDA-CAC are described in our previous article [25]. Then, the magnetite nanoparticles (Fe_3O_4NPs) were *in situ* produced onto the GO-EDA-CAC surface through the well-known co-precipitation

method, which requires the use of both ferric and ferrous ions in basic conditions [29]. First, the formation of the Fe_3O_4NPs onto the GO-EDA-CAC surface was qualitatively evidenced by FTIR analysis **(Fig. S3a†).** Indeed, the FTIR spectrum of the GO-EDA-CAC@Fe_3O_4NPs **(Fig. S3a†)** displays a peak at 635 cm^{-1} which may be attributed to the stretching vibrations of the CH_2-Cl groups and another one located in the range 620-598 cm^{-1} that is characteristic of octahedral and tetrahedral stretching vibrations of the Fe-O bonds in Fe_3O_4NPs [5].

The immobilization of Fe_3O_4NPs onto the GO-based material surface was also demonstrated by analyzing both the elemental composition of (GO-EDA-CAC)@Fe_3O_4NPs by EDX **(Fig. 1a)** and its morphology by SEM **(Fig. 1b).**

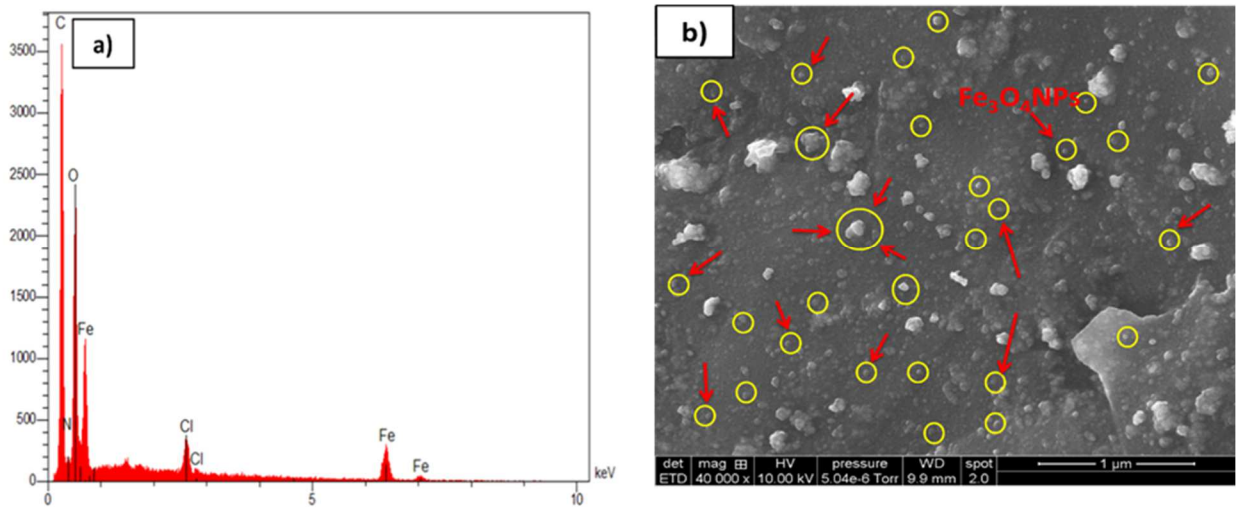

Figure 1. **(a)** EDX spectrum and **(b)** SEM image of GO-EDA-CAC@Fe_3O_4NPs.

Fig. 1a shows the EDX spectrum of GO-EDA-CAC@Fe_3O_4NPs, which mostly displays the presence of carbon, nitrogen, oxygen, chlorine, and iron, as expected. In addition, the SEM image of GO-EDA-CAC@Fe_3O_4NPs **(Fig.1b)** shows the presence of sphere-like structures with diameters ranging from 6 nm to 20 nm. A few larger aggregates with an average diameter centered at 80 nm are also observed.

Then, the weight content of magnetite nanoparticles in the (GO-EDA-CAC)@Fe_3O_4NPs was estimated by thermogravimetric analysis (TGA) **(Fig. S4a†)** and it was calculated to be around 28wt % when compared to the curve of GO-EDA-CAC [25].

3.1.2. Grafting of BPED onto GO-EDA-CAC@Fe_3O_4NPs

The grafting of BPED groups onto the GO-EDA-CAC@Fe_3O_4NPs surface was performed according to the experimental procedure described by Laroussi *et al.,* [25] and it was characterized by X-ray photoelectron spectroscopy (XPS). The XPS spectra of C 1s and N 1s for (GO-EDA-CAC)@Fe_3O_4NPs and [(GO-EDA-CAC)@Fe_3O_4NPs]-BPED materials are shown in **Fig. S5†** and **Fig. S6†**, respectively. Each individual peak of carbon and nitrogen functional groups was fitted with a Gaussian function and their peak area ratios were calculated **(Table S2† and Table S3†)**. The C 1S spectrum of GO-EDA-CAC exhibits different peaks at 285.45 eV, 286.85 eV, 287.95 eV and 289.12 eV corresponding to C=C/C-C, C-N, O-C-O and C=O bonds, respectively, **(Fig. S5†)** while the peak intensity of carbon atoms bonded to nitrogen increases after BPED grafting, as expected **(Fig. S6†).** In addition, the C-N species ratio content increases from 18.7% for GO-EDA-CAC@Fe_3O_4NPs to 32.5% for [(GO-EDA-CAC)@Fe_3O_4NPs]-BPED **(Table S2†)**. Furthermore, the high-resolution N 1s spectrum of (GO-EDA-CAC)@Fe_3O_4NPs **(Fig. S6a†)** displays three peaks centered at 400.11 eV (C=N), 400.18 eV (C-NR_2) and 401.74 eV (N-C=O) and the amounts of C=N- (13.7%) and O=C-N (12.9%) **(Table S3†)** increase when compared to those of the (GO-EDA-CAC)@Fe_3O_4NPs which attest for the successful grafting of BPED groups onto the (GO-EDA-CAC)@Fe_3O_4NPs.

Moreover, the presence of BPED groups onto the GO-EDA-CAC@Fe_3O_4NPs was quantitatively studied by TGA and it was observed an increase of the weight loss of 10% in comparison with the TGA curve of GO-EDA-CAC@Fe_3O_4NPs **(Fig. S4a†).** To obtain more understanding of the effect of the grafting of BPED groups onto the morphology of the (GO-

EDA-CAC)@Fe_3O_4NPs surface, scanning electron microscopy (SEM) was also conducted. However, no significant change was observed upon BPED grafting **(Fig. S7†).**

The XRD patterns of [GO-EDA-CAC)@Fe_3O_4NPs]-BPED is shown in **Fig. 2**.

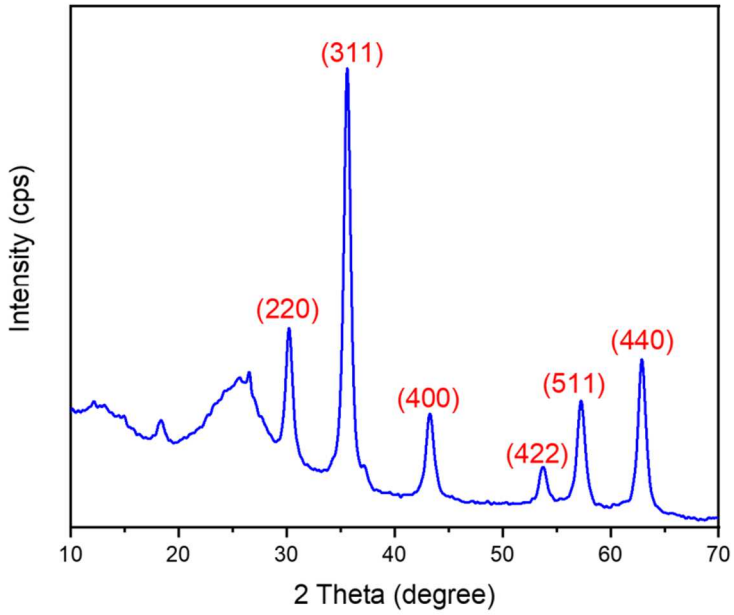

Figure 2. XRD patterns of [(GO-EDA-CAC)@Fe_3O_4NPs]-BPED.

As it can be seen, the broad peak at 2Θ= 25.12° may be attributed to the presence of multi-functional groups such as amine, amide and pyridine moieties located onto the GO sheets while the characteristic diffraction peaks of Fe_3O_4NPs are observed at 2Θ= 31.19°, 35.61°, 43.25°, 54.47°, 57.41°, and 62.95°, corresponding to (220), (311), (400), (422), (511), and (440) crystal plane, respectively [5].

Then, the size of Fe_3O_4NPs was estimated from the full-width at half maximum of the most intense diffraction peak by Scherrer's equation (Eq.2) [44]:

$$D = \frac{K\,\lambda}{\beta\,cos\theta} \qquad \textbf{(2)}$$

Where K is the grain shape factor (k= 0.89), λ is the wavelength of CuK_α radiation (λ = 0.15406 nm), β is the Full-Width at half maximum of the most intense diffraction peak (311) in the 2Θ scale and Θ is the Bragg's angle. Using **Eq.2,** we obtained a diameter of 6.00 nm, which is in the same size range that the one observed by the SEM image.

In addition, the magnetization proprieties of [GO-EDA-CAC@Fe_3O_4NPs]-BPED were studied at 300 K and the plots of magnetization (M) versus magnetic field (H) are shown in **Fig. 3a**.

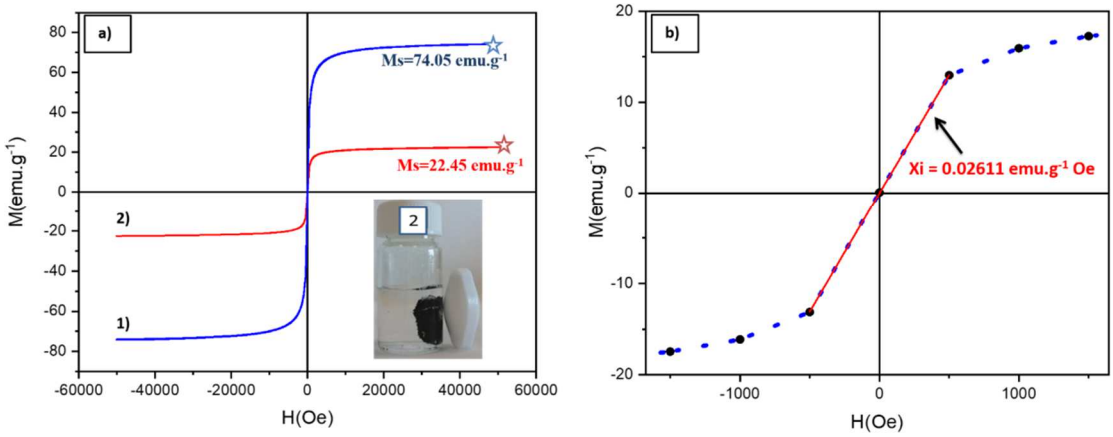

Figure 3. (a) Magnetization (M) versus magnetic field (H) recorded at 300K for **(1)** Fe_3O_4NPs and **(2)** [GO-EDA-CAC)@Fe_3O_4NPs]-BPED. **(b)** Susceptibility of [GO-EDA-CAC@Fe_3O_4NPs]-BPED **(2)**, when magnetic field is near zero.

No coercivity or hysteresis can be observed in the magnetization curves, indicating that the [GO-EDA-CAC@Fe_3O_4NPs]-BPED is superparamagnetic. In addition, the saturation magnetization (M_s) of [GO-EDA-CAC@Fe_3O_4NPs]-BPED (22.45 emu.g^{-1}) is lower than that of the Fe_3O_4NPs (74.05 emu.g^{-1}) which may be due to the presence of non-magnetic GO sheets and the smaller size of the supported Fe_3O_4NPs [45]. On the other hand, it is observed

from the inset in **Fig. 3a** that the [GO-EDA-CAC@Fe_3O_4NPs]-BPED material can be easily isolated by applying an external magnetic field.

In case of almost zero coercivity (M_c) and zero remanence (M_r), the average size (D_m) of the Fe_3O_4NPs can be calculated from the initial susceptibility (x_i) using Eq.3 [46]:

$$D_m = \sqrt{\frac{18\times K\times T\times x_i}{\Pi\times\rho\times(M_S)^2}} \quad \textbf{(3)}$$

Where K is Boltzmann constant, T is the temperature (300 K), x_i is the susceptibility when the magnetic field is near zero (0.02611 emu.g^{-1}.Oe) **(Fig. 3b)**, ρ is the density of magnetite nanoparticles, M_s is the saturation magnetization. Assuming that the saturation magnetization (M_s) corresponds to that of the [GO-EDA-CAC@Fe_3O_4NPs]-BPED (22.45 emu.g^{-1}), it was calculated a diameter of 6.01 nm which in good agreement with the results obtained from calculated the Scherrer's equation (XRD) **(Eq.2)** and nearly in the range of the ones evaluated from the SEM image **(Fig. S7†).**

Moreover, **Fig.4** shows the Zero field cooled (ZFC) and field cooled (FC) magnetization of [GO-EDA-CAC@Fe_3O_4NPs-BPED] as a function of temperature. It can be observed that both ZFC and FC curves of the [GO-EDA-CAC@Fe_3O_4NPs-BPED] absorbent have the same magnetization behavior for temperature higher than 88K (**Fig.4)**. The maximum of the ZFC curve is called the blocking temperature (Tb) of Fe3O4NPs that can be also calculated by using Eq.4 [47]:

$$Tb=(\beta\times K\times Vm)/(k\_b\times\ln(\tau_m/\tau\_0)) \quad \textbf{(4)}$$

Where β is a constant depending on the crystal size distribution (β=9.2), K is the anisotropy constant of the crystal (K= 5×104 J m^{-3}), Vm is the crystal volume (1.125×10^{-26}m^3), kb is the Boltzmann constant (kb = 1,380 649 × 10−23 J K^{-1}), τ_m is the measurement time and τ_0 is a characteristic relaxation time of crystal of 10^{-11} s [47].

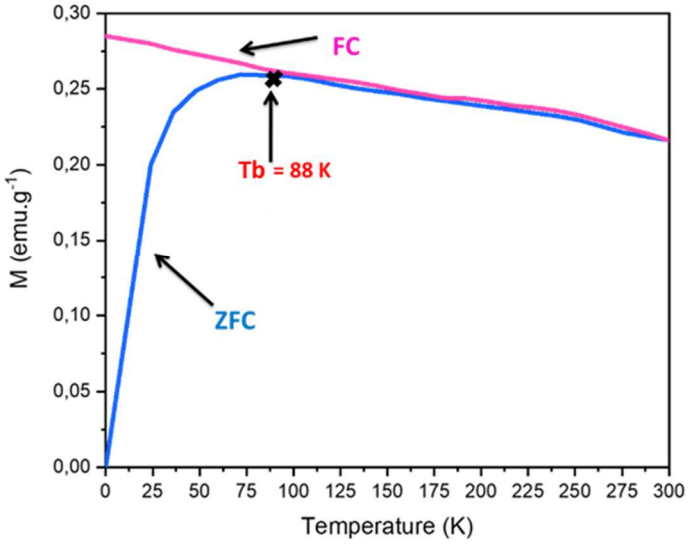

Figure 4. ZFC (Zero field cooled) and FC (Field cooled) temperature dependence of magnetic susceptibility for [(GO-EDA-CAC)@Fe_3O_4NPS]-BPED.

A value of 87.67 K was calculated for Tb, which is close to the experimental one (88 K ; **Fig.4).** The blocking temperature (T_b) of the [(GO-EDA-CAC)@Fe_3O_4NPs]-BPED (88 K) is lower than that of the Fe_3O_4NPs (226 K) [48] which may be explained by the increase of inter-distance between Fe_3O_4NPs and consequently a decrease of dipole-dipole interactions.

3.2. Effect of the pH and the contact time on Cu(II) ions adsorption by GO-EDA-CAC@Fe_3O_4NPs and [GO-EDA-CAC@Fe_3O_4NPs]-BPED

3.2.1. Effect of the pH onto Cu (II) adsorption capacities and zero-point charge (pH zpc) studies

The pH of the metal ions containing aqueous solutions is a key parameter for the obtained adsorption capacity, as reported by several authors in the literature [49]. Herein, we investigated the pH range 4.0-8.0 and a blank experiment without the GO-based absorbent was also performed in order to check the precipitation of Cu(II) ions, as illustrated in **Fig. S8**†. As it can be observed, the Cu(II) ions adsorption capacities increase with increasing the pH from 4 to 8 whatever the GO-based absorbent and the adsorption capacities are higher for

the GO-EDA-CAC@Fe3O4NPs]-BPED. The low Cu(II) adsorption capacities obtained in acidic experimental conditions may be explained by the positive surface charge of the absorbents at low pH and the protonation of the BPED groups for the GO-EDA-CAC@Fe3O4NPs]-BPED absorbent which partly prevent Cu(II) ions from adsorption. Indeed, the pH point zero charge (pH_{pzc}) of the adsorbents were determined to evaluate their surface charges and the experimental curves (plots of $pH_{(Final)}$ *vs* $pH_{(Initial)}$) are shown in **Fig. S9†**. It is expected that the surface of adsorbent becomes negatively charged when the pH of the aqueous solution is higher than pH_{pzc} leading to favorable electrostatic interactions with Cu(II) ions [49, 50] and we obtained a pH_{pzc} of 6.6 for the GO-EDA-CAC@Fe_3O_4NPs absorbent and a pH_{pzc} of 6.9 for the [GO-EDA-CAC@Fe_3O_4NPs]-BPED one. Accordingly, the higher adsorption capcity ($Q_{Cu(II)}$) is achieved at pH=7 for the [(GO-EDA-CAC)@Fe_3O_4NPs]-BPED adsorbent with a value of 3.808±0.125 $mmol.g^{-1}$ which is slightly higher than the one of GO-EDA-CAC-BPED ($Q_{(Cu(II))}$= 3.464±0.100 $mmol.g^{-1}$).

3.2.2. Effect of the contact time on the Cu(II) ions adsorption capacities

The adsorption of Cu(II) ions at different contact times were performed with a Cu(II) ion concentration of 250 $mg.L^{-1}$ at pH=7 for GO-EDA-CAC)@Fe_3O_4NPs and [GO-EDA-CAC)@Fe_3O_4NPs]-BPED absorbents (**Fig. S10†).** As it can been seen, the optimal contact time depends on the nature of the adsorbent and the optimal contact time is 5h for (GO-EDA CAC)@Fe_3O_4NPs and 3h for [(GO-EDA-CAC)@Fe_3O_4NPs]-BPED. Thus, the [(GO-EDA-CAC)@Fe_3O_4NPs]-BPED absorbent achieves an equilibrium adsorption faster than the GO-EDA CAC@Fe_3O_4NPs one and other GO-based adsorbents (GO, GO-EDA, GO-EDA-CAC, and GO-EDA-CAC-BPED) that were studied in our previous work [25]. This could be ascribed to a higher number of active sites (e.g. BPED groups) located onto the [(GO-EDA-CAC)@Fe_3O_4NPs]-BPED sheets.

3.3. Adsorption kinetics

Four kinetics models, including, the pseudo-first-order [51], the pseudo-second-order [52], the Roginsky-Zeldovich [53] and the intra-particle diffusion [54] ones were used to fit the experimental data and to understand both the adsorption process and the diffusion of the Cu(II) adsorbate through adsorbent pores. The linear forms of these models are described in supporting information **(Section 2)**. Linear fitting plots of pseudo-first-order and pseudo-second-order models are shown in **Fig. 5** and the usual calculated parameters from these models are summarized in **table 1.**

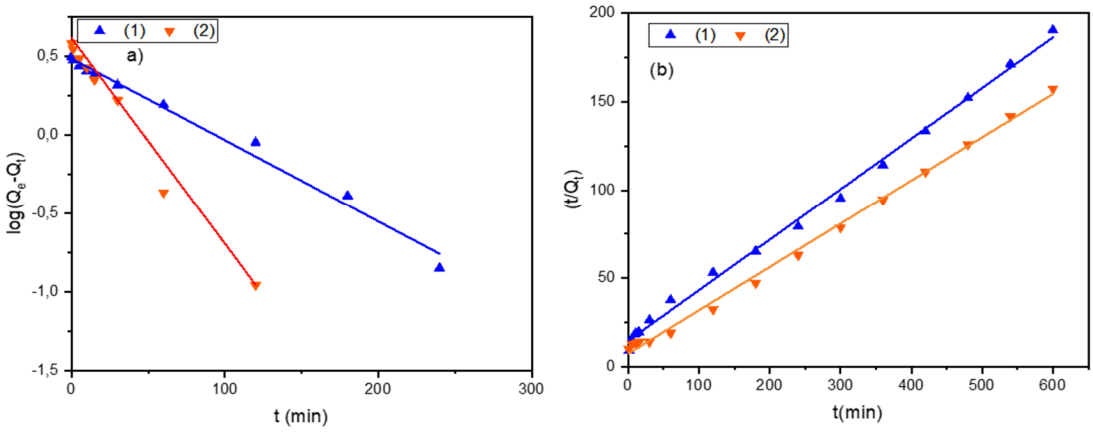

Figure 5. (a) Pseudo-first-order and **(b)** Pseudo-second-order kinetics plots for adsorption of Cu(II) ions onto **(1)** GO-EDA-CAC@Fe_3O_4NPs and **(2)** [GO-EDA-CAC@Fe_3O_4NPs]-BPED.

According to the correlation coefficient values, it is demonstrated that the adsorption data fit better with the pseudo-second-order model than with the pseudo-first-order model while the calculated Q_e **(Table 1)** are close to the experimental ones (in the range 3.5-3.8 $mmol.g^{-1}$). Thus, the adsorption of Cu(II) ions onto magnetic adsorbents is controlled by a chemical sorption which includes exchange electrons between adsorbent and Cu(II) ions [55].

Table 1. Usual calculated parameters calculated from the pseudo-first-order kinetic, the pseudo-second-order kinetic, the Roginsky-Zeldovich model and the intra-particle diffusion kinetic models for the adsorption of Cu (II) ions onto **(1)** (GO-EDA-CAC)@Fe_3O_4NPs and **(2)** [(GO-EDA-CAC)@Fe_3O_4NPs]-BPED.

Models	Parameters	Adsorbents	
		1	**2**
First-order Kinetic model	R^2	0.990	0.985
	$K_1 \times 10^2$ (min^{-1})	1.151±0.002	3.477±0.002
	$Q_{e,\,cal}$ ($mmol.g^{-1}$)	3.054±0.021	4.027±0.011
Second-order Kinetic model	R^2	0.996	0.998
	$K_2 \times 10^2$ ($g.mmol^{-1}.min^{-1}$)	0.697±0.005	0.211±0.004
	$Q_{e,\,cal}$ ($mmol.g^{-1}$)	3.125±0.007	3.817±0.005
Roginsky-Zeldovich model	R^2	0.939	0.923
	α ($mmol.g^{-1}.min^{-1}$)	0.258±0.197	0.717±0.272
	β ($g.mmol^{-1}$)	1.712±0.041	1.557±0.057
The intraparticle diffusion Kinetic	R^2	0.998	0.997
	Ki_1 ($mmol.g^{-1}.min^{-1/2}$)	0.208±0.003	0.403±0.047
	L_1 ($mmol.g^{-1}.min^{-1/2}$)	-0.043±0.017	-0.070±0.202
	R^2	0.992	0.991
	Ki_2 ($mmol.g^{-1}.min^{-1/2}$)	0.093±0.008	0.127±0.047
	L_2 ($mmol.g^{-1}.min^{-1/2}$)	1.578±0.127	2.803±0.051

The experimental data were also fitted with the Roginsky-Zeldovich model by using **Eq. 3**, (S.I†) and the corresponding calculated parameters are summarized in **Table 1**. In particular, the low values of α suggest a fast equilibrium adsorption and a low activation energy for the chemsorption [56].

In order to investigate the mechanism of the adsorption of Cu(II) ions onto the different adsorbents, the kinetic results were also fitted with the intra-particle diffusion model by using **Eq. 4,** (S.I†) and the corresponding calculated parameters are listed in **Table 1**. Considering these latter results, **Fig. 6** shows a multi-linear fit of the intraparticle diffusion model for the adsorption of Cu(II) ions onto (GO-EDA-CAC)@Fe_3O_4NPs and [(GO-EDA-CAC)@Fe_3O_4NPs]-BPED.

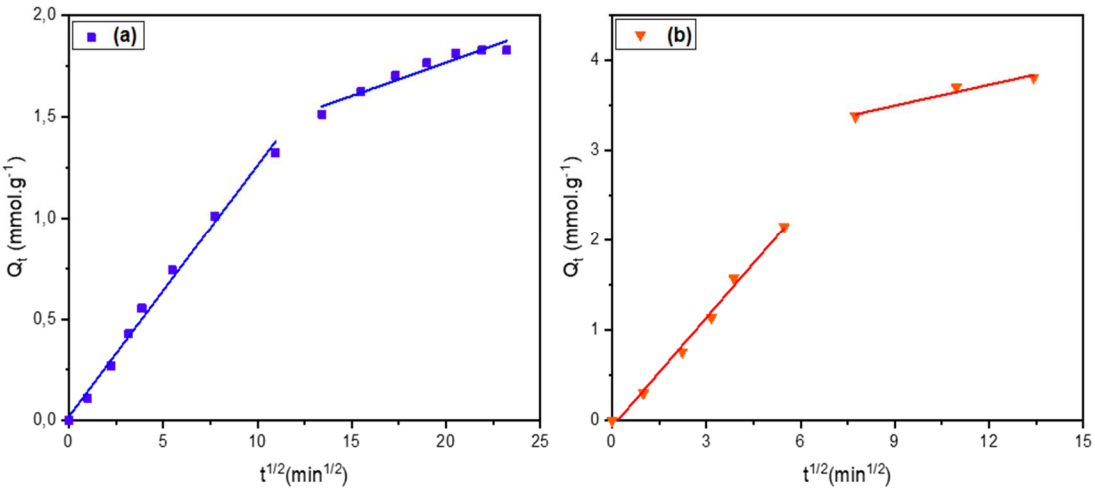

Figure 6. Adsorption capacities versus $t^{1/2}$ calculated from the intra-particle diffusion kinetic model for the adsorption of Cu(II) ions by the adsorbents **(a)** (GO-EDA-CAC)@Fe_3O_4NPs and **(b)** [(GO-EDA-CAC)@Fe_3O_4NPs]-BPED.

For both the adsorbents, the first linear stage corresponds to the diffusion of the Cu(II) ions onto the surface of the magnetic adsorbent. The second linear stage describes the gradual adsorption stage which may be attributed to the diffusion of Cu(II) ions inside the active sites of the adsorbent and the beginning of saturation**.** Moreover, the intra-particle diffusion constants show K_{i1} (first stage) is higher than K_{i2} (second stage) **(Table 1)**, indicating that the second stage corresponds to a slower transport of Cu(II) ions from the liquid phase up to the active sites of the adsorbent during the adsorption process.

3.4. Homo-coupling study of terminal alkynes in the presence of reused [(GO-EDA-CAC)@Fe_3O_4NPs]-BPED-Cu(II), as supported catalyst

The recyclability of the [GO-EDA-CAC@Fe_3O_4NPs]-BPED-Cu(II) material is of great interest in particular for the catalysis of organic reactions such as homocoupling of alkynes. Indeed, the synthesis of 1,3-diynes through the homocoupling of alkynes requires the use of metal catalysts such as palladium which is efficient at low loading but the price of this precious metal has led to the use of a low-cost metal catalyst such as copper [57]. Therefore, we investigated the use of [GO-EDA-CAC@Fe_3O_4NPs]-Cu(II) and [GO-EDA-CAC@Fe_3O_4NPs]-BPED-Cu(II) as supported catalysts for the homocoulping of phenylacetylene.

3.4.1. Effect of the catalyst nature, the solvent, the temperature and the base on the homocoupling reaction of phenylacetylene

In this study, the homocoupling of phenylacetylene was selected as a model reaction to evaluate the catalytic activity of the Cu(II) ions adsorbed onto the magnetic GO-based adsorbents and in order to find the optimal experimental conditions. For comparison, the homocoupling of phenylacetylene was first carried out in the presence of both usual unsupported and supported copper catalysts with EtOH as solvent and Et_3N as a base in air at 80 °C. It should be noted that the weight content of copper ions located onto the [GO-EDA-CAC@Fe3O4NPs]-BPED and [GO-EDA-CAC@Fe3O4NPs] are 0.24g/g and 0.22g/g, respectively and corresponding to adsorption capacities of 3.8 $mmol.g^{-1}$ and 3.5 $mmol.g^{-1}$, respectively. Arbitrarily, we have used all the recovered Cu(II)-GO-based substrates from the adsorption experiment (about 10 mg per experiment) as supported catalysts for the homocoupling of alkyne and it was compared to experiments containing a copper ions amount of 4mg that is usually used for this reaction [35, 36]. The results are summarized in **Fig. 7**.

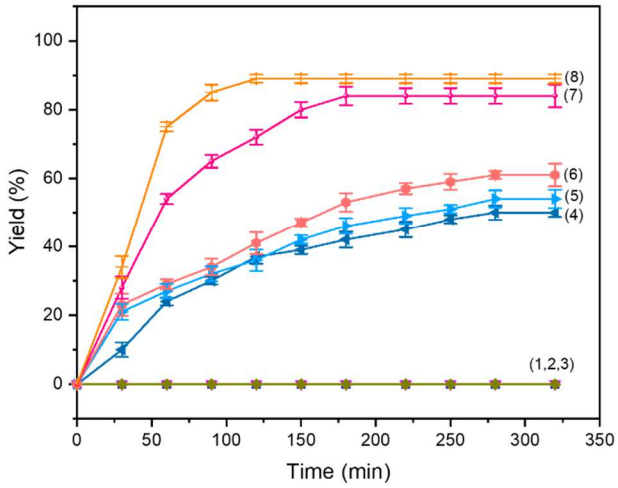

Figure 7. Effect of the different catalysts on the time-yield plot for the homocoupling of phenylacetylene: **(1)** without any catalyst, **(2)** with (GO-EDA-CAC)@Fe_3O_4NPs (10 mg), **(3)** with [(GO-EDA-CAC)@Fe_3O_4NPs]-BPED (10 mg), **(4)** with CuI (4 mg), **(5)** with $CuBr_2$ (4 mg), **(6)** with $CuCl_2$ (4 mg), **(7)** with (GO-EDA-CAC)@Fe_3O_4NPs-Cu(II) (10 mg ; 2.2 mg Cu(II)) and **(8)** with [(GO-EDA-CAC)@Fe_3O_4NPs]-BPED-Cu(II) (10 mg ; 2.4 mg Cu(II)). Experimental conditions: phenylacetylene (1.0 mmol, 1.0 eq.), Et_3N (1.2 mmol, 1.2 eq.), and EtOH (1.0 mL) at 80 °C under air, the error bars correspond to one standard deviation n=2.

As it can be seen, the homocoupling reaction of phenylacetylene is not efficient without any catalyst though in the presence of GO-EDA-CAC@Fe_3O_4NPs and GO-EDA-CAC)@Fe_3O_4NPs-BPED substrates, as expected. For the copper-based catalysts, we observe the presence of a plateau corresponding to the higher reaction yield that can be obtained at 100% phenylacetylene conversion (determined by gas chromatography) due to the selectivity of the homocoupling reaction (presence of secondary products). The CuX_2 (X: Cl, Br) unsupported catalysts are more efficient than the CuI one for reaction times higher than 150 minutes with a maximum reaction yield of 61% after 280 minutes suggesting that Cu(II) ions play a key role in the homocoupling reaction. Moreover, despite their lower Cu(II) weight content (about 2 fold lower), the supported copper catalysts such as (GO-EDA-CAC)@Fe_3O_4NPs-Cu(II) and [(GO-EDA-CAC)@Fe_3O_4NPs]-BPED-Cu(II) lead to higher

yields in a shorter time. Indeed, we obtained homocoupling yields in the range 80-90 % for reaction times lower than 180 min **(Fig. 7)**. The latter behavior may be due to the high Cu(II)-GO-based suspension stability in glycerol and especially to the easier coordination of the penylacetylene reactant onto the Cu(II) ions adsorbed onto the GO-based surface, as discussed in 3.4.3. (S**cheme 2**). Moroever, it is observed that the time necessary to produce the 1,4-diphenylbuta-1,3-diyne depends on the amount of Cu(II) ions that is adsorbed onto the GO-based surface, so that it is 180 min for (GO-EDA CAC)@Fe_3O_4NPs-Cu(II) and 120 min for [(GO-EDA-CAC)@Fe_3O_4NPs]-BPED-Cu(II). Then, the influence of the solvent onto the homocoupling reaction yield was studied and the results are summerized in **Table 2**.

Table 2. Effect of the solvent on the time-yield plot for the homocoupling of phenylacetylene in presence of [GO-EDA-CAC@Fe_3O_4NPs]-BPED-Cu(II).

Solvents	**Yields (%)[a]**
THF	15±1
DMF	25±1
DMSO	45±1
n-propanol	62±1
Methanol	74±2
Ethanol	89±1
Glycerol	94±1

[a]Experimental conditions: Phenylacetylene (1.0 mmol, 1.0 eq.), Et_3N (1.2 mmol, 1.2 eq.), [GO-EDA-CAC@Fe_3O_4NPs]-BPED-Cu(II) (10 mg), and solvent (1.0 mL) at 80 °C under air for 120 min; the error bars correspond to one standard deviation n=2.

It can be concluded that the use of polar aprotic solvents do not permit to obtain an homocoupling reaction yield higher than 60% for reaction time higher than 100 min. In contrast, the use of polar protic solvents, such as *n*-propanol and ethanol, leads to a homocoupling reaction yield increasing from 62% to 89%, respectively, for a reaction time of 120 min **(Table 2)**. Moreover, to improve the greenness of the homocoupling reaction, it was

also carried out in a biocompatible and non-flammable solvent such as glycerol, and we obtained an excellent yield of 94±0.62% for a reaction time of 120 min. Therefore, to investigate the effect of temperature on the homocoupling reaction of phenylacetylene under the most greener experimental conditions, glycerol was selected as the most suitable solvent and the reaction was performed in a low temperature range (40-80°C ; **Fig. 8).** It should be also mentioned that the homocoupling reaction of alkynes requires the use of low temperatures to avoid the presence of side reactions that is why a temperature of 80°C is often used [35, 36, 58, 59].

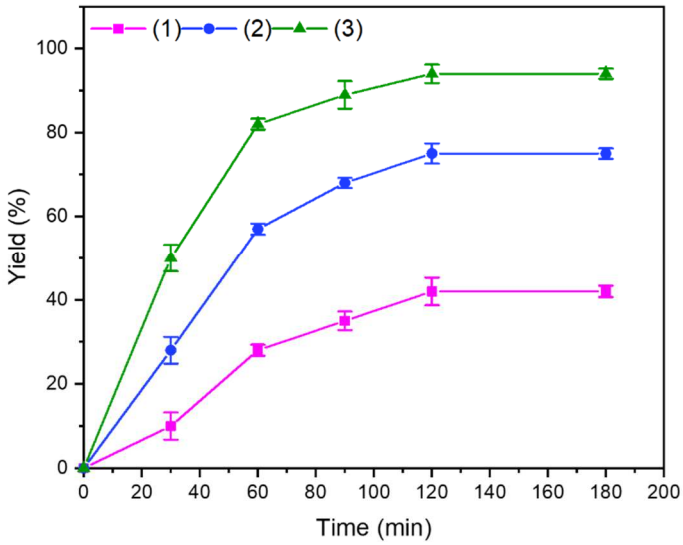

Figure 8. Effect of temperature on the time-yield plot for the homocoupling reaction: **(1)** 40 °C, **(2)** 60 °C, and **(3)** 80 °C. Experimental conditions: Phenylacetylene (1.0 mmol, 1.0 eq.), Et_3N (1.2 mmol, 1.2 eq.), [(GO-EDA-CAC)@Fe_3O_4NPs]-BPED-Cu(II) (10 mg), and glycerol (1.0 mL); the error bars correspond to one standard deviation n=2.

Fig. 8 shows that the reaction yield increases by increasing both the reaction time and the temperature and the highest yield is as high as 94% and was achieved at 80 °C for 120 min. Thus, 80 °C was selected as the optimum temperature for studying the effect of the base nature onto the reaction yield.

Table 3 summarized the results obtained with the use of some common organic and inorganic bases under identical experimental conditions.

Table 3. Effect of the base nature on the time-yield plot for the homocoupling of phenylacetylene.

Bases	**Yields (%)[b]**
Without base	0
n-butylamine	35±1
Diisopropylamine	45±1
Diethylamine	69±1
Triethylamine	94±1
$CaCO_3$	90±1
$K_3PO_4.3H_2O$	92±1
Na_2CO_3	99±1

[b] Experimental conditions: Phenylacetylene (1.0 mmol, 1.0 eq.), base (1.2 mmol, 1.2 eq.), [(GO-EDA-CAC)@Fe_3O_4NPs]-BPED-Cu(II) (10 mg), and glycerol (1.0 mL) at 80 °C under air for 120 min; the error bars correspond to one standard deviation n=2.

As expected, the reaction could not be performed without any base and most of the organic bases including *tert*-butylamine, diethylamine, and diisopropylamine gave poor yields (< 65 %) for a reaction time of 120 min. Triethylamine was the most efficient organic base with a yield of 94±0.62% for 120min. In comparison, the inorganic bases including $CaCO_3$ and $K_3PO_4.3H_2O$ lead to higher yields, especially Na_2CO_3 with a yield to 99%. Thus, the optimal greener experimental conditions for the homocoupling of phenylacetylene are based on the use of 10 mg of [GO-EDA-CAC)@Fe_3O_4NPs]-BPED-Cu(II) in glycerol at 80 °C, in presence Na_2CO_3 as a base. In this regard, it is interesting to measure the green performance of the homocoupling reaction so that we have calculated some green metrics [60] such as :

-the *E*-factor, defined by the ratio of the total mass of waste generated in the synthetic scheme to the mass of product isolated **(Eq. 5)**

$$E\sim\text{factor} = \frac{\sum \text{mass of wastes}}{\text{mass of isolated product}} \quad \textbf{(5)}$$

-the Process Mass Intensity (PMI), defined as the ratio of the total mass of materials to the mass of the isolated product **(Eq. 6)**

$$\text{PMI} = \frac{\sum \text{mass of materials}}{\text{mass of isolated product}} = E + 1 \quad \textbf{(6)}$$

-the Atom Economy (AE), defined as the number of atoms from the starting materials that are incorporated into the final product **(Eq. 7)**

$$\text{Atom economy (\%)} = \frac{\text{Molecular weight of desired product}}{\sum \text{ Molecular weight of reactants}} \times 100 \quad \textbf{(7)}$$

Moreover, an alternative mass-based metric such as the Reaction Mass Efficiency is usually discussed and is defined as the percentage of actual mass of desire product to the mass of all reactants used. It takes into account both atom economy and chemical yield **(Eq. 8)**

$$\text{Reaction mass efficiency (\%)} = \frac{\text{mass of desired product}}{\text{mass of all reactants}} \times 100 \quad \textbf{(8)}$$

The results are summarized in **Table 4**.

Table 4. Evaluation of green chemistry metrics for the synthesis of a 1,3-diyne based on phenylacetylene.

	Reactant (Phenylacetylene)	**Solvent** (Glycerol)	**Base** (Na_2CO_3)	**Auxiliary**	**Product**
Mass	1.02 g	12.6 g	1.27 g	----	1.01 g
Number of moles	0.010 mol	----	0.012 mol	----	0.005 mol
Molecular mass	102.05 $g.mol^{-1}$	----	105.98 $g.mol^{-1}$	----	202.07 $g.mol^{-1}$
			Values		
E-factor			13.74 Kg waste/Kg product		
Process Mass Intensity			14.74 kg waste/Kg product		
Atom economy			97.1%		
Reaction mass efficiency			99.0%		

According to these results, we can conclude that our experimental conditions can enable the synthesis of symmetrical conjugated 1,3-diynes at a large scale with an *E*-factor of 13.74 Kg/ 1 kg product, 97.13% of atom economy and a reaction mass efficiency of 99.0% **(Table 4)**. Therefore, these results are more interesting than the ones published elsewhere (*E*-factor of 53.51 Kg, PMI = 54.51 Kg/Kg, AE = 78.85%, and RME = 99.0% **(Table S3†)** [61]**.**

3.4.2. Scope and limitation of the Glaser homocoupling reaction

Considering the efficiency of the experimental conditions described above, the homocoupling of other phenylacetylene-based molecules containing electron-donating groups and electron-withdrawing groups was studied (**Fig. 9**).

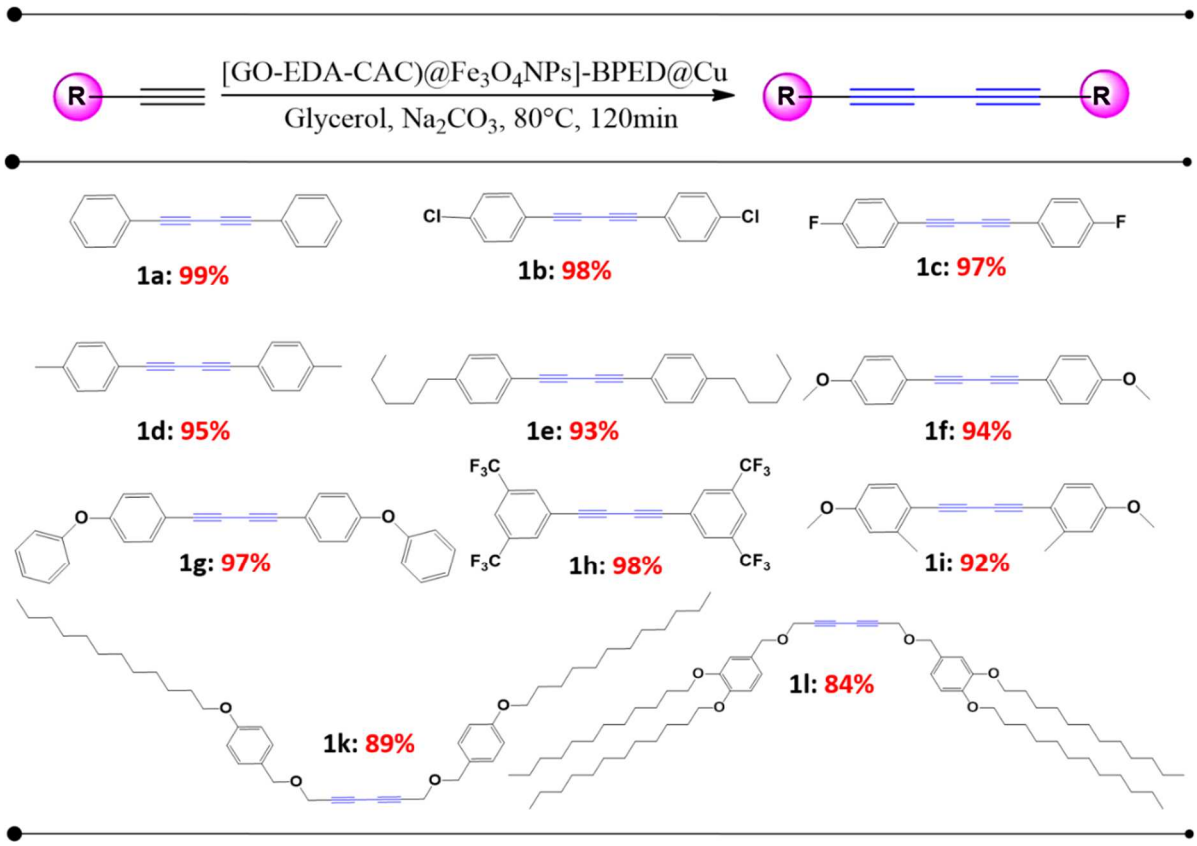

[a]Experimental conditions: Phenylacetylene (1.0mmol, 1.0 eq.), Na_2CO_3 (1.2 mmol, 1.2 eq.), [GO-EDA-CAC@Fe_3O_4NPs]-BPED-Cu(II) (10mg), and glycerol (1.0 mL) at 80 °C under air.

Figure 9. Symmetric dialkynes synthesized in presence of [GO-EDA-CAC@Fe_3O_4NPs]-BPED-Cu(II)[a]

The phenylacetylenes having chloro **(1b)** and fluoro **(1c)** atoms in *para*-positions and trifluoromethyl groups **(1h)** in meta positions gave the higher yields, close to 98% (**Fig.9**) while the presence of electron-donating substituents such as *p*-methyl **(1d)** and *p*-propyl **(1e)** onto phenylacetylene did not affect the homocoupling yield. Finally, we have checked the efficiency of the homocoupling reaction onto etheroxide-based alkynes and we also obtained high yields (89% for **(1k)** and 84% for **(1l), Fig.9)**.

All these results confirmed that the [GO-EDA-CAC)@Fe_3O_4NPs]-BPED-Cu(II) can be recycled as a supported catalyst for the homocoupling reaction of terminal alkynes.

3.4.3. Mechanistic scheme for the homocoupling of terminal alkynes in the presence of [GO-EDA-CAC@Fe_3O_4NPs]-BPED-Cu(II)

According to the literature [62-65] and this work a proposal for the mechanism of the preparation of 1,3-diyne derivatives in presence of [(GO-EDA-CAC)@Fe_3O_4NPs]-BPED-Cu(II) as catalyst is shown in **Scheme 2.**

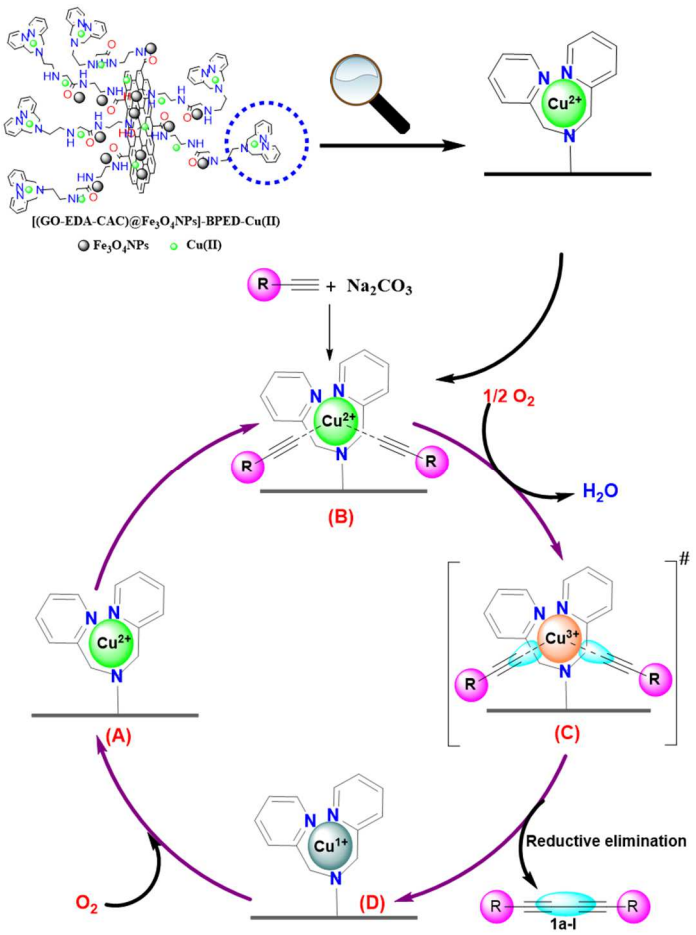

Scheme 2. A plausible mechanism for the [(GO-EDA-CAC)@Fe_3O_4NPs]-BPED-Cu(II) catalyzed homocoupling of terminal alkynes.

In the initial step, the acetylene group is deprotonated in presence of the alkaline conditions of Na_2CO_3. Then, it is expected that the high surface area of the GO-based adsorbent and the high number of coordination sites for Cu(II) ions will facilitate the *in situ* formation of complexes Cu(II)-acetylide **(B)**. In the second step, the air oxidation of Cu(II) **(B)** leads to the formation of the instable intermediate Cu(III) **(C)** whose decomposition allows the production of the 1,3-diyne product **(D)** through a spontaneous reduction [62]**.** In the last step, the reduced Cu(I) species are oxidized to Cu(II) and ensures the regeneration of the catalyst.

3.4.4. Regeneration/reusability

Regeneration of the catalyst is a key parameter when assessing for commercial applications. The reusability of the supported [GO-EDA-CAC@Fe_3O_4NPs]-BPED-Cu(II) catalyst for the homocoupling reaction was investigated with phenylacetylene as a model molecule under our optimal experimental conditions. After completion of the reaction, the catalyst was efficiently separated from the reaction media by using an external magnetic field after each experiment. Then, the recovered catalyst was washed with methanol several times and dried carefully before reuse in the next experiment (Figure 10).

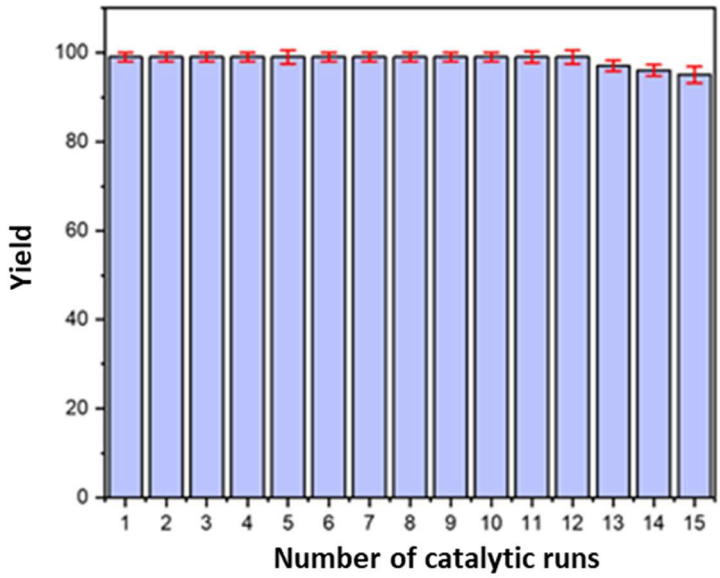

Figure. 10. Number of the catalytic runs for the homocouplig reaction of phenylacetylene in presence of [(GO-EDA-CAC)@Fe_3O_4NPs]-BPED-Cu(II). Experimental conditions: Phenylacetylene (1.0mmol, 1.0 eq.), Na_2CO_3 (1.2 mmol, 1.2 eq.), and glycerol (1.0 mL) at 80 °C under air for 120 min.

As shown in **Fig. 10,** the recovered catalyst was consecutively reused for fifteen runs without a significant loss of its activity. It should be mentioned that the FTIR spectrum of the reused [(GO-EDA-CAC)@Fe3O4NPs]-BPED-Cu(II) after fifteen runs (Fig.S11b†) still contains the typical absorption band of the Cu-bond at 453 cm-1 while no significant differences are

observed between the positions of both the stretching vibrations and the absorption bands of the samples before and after fifteen catalytic runs (Fig.S11†).

In another experiment, the homo-coupling reaction was performed under our optimal experimental conditions but the catalyst was quickly recovered from the hot solution after 60 min. After the removal of the [(GO-EDA-CAC)@Fe_3O_4NPs]-BPED-Cu(II) material, **Figure 11** demonstrates that the homocoupling reaction do not show any significant progress, as expected. In addition, the reaction mixture was analyzed using ICP-MS to determine the supernatant content of probably leached Cu(II) in the solution. Nevertheless, no significant amount of Cu(II) was detected in the mixture, demonstrating that the designed [(GO-EDA-CAC)@Fe_3O_4NPs]-BPED material exhibits active ligand sites for Cu(II) ions.

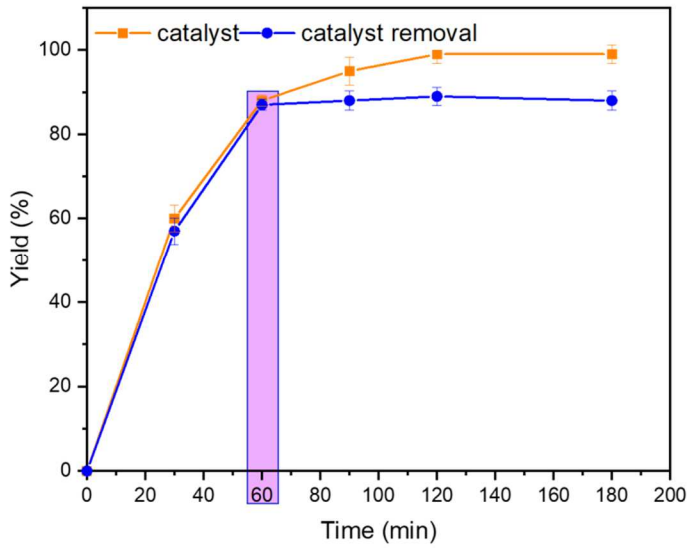

Figure 11. Influence of the removal of the [(GO-EDA-CAC)@Fe_3O_4NPs]-BPED-Cu(II) onto the homocoupling yield of phenylacetylene.

3.4.5. Influence of different catalysts onto the homocoupling of phenylacetylene

A comparison between the catalytic activity of the [GO-EDA-CAC@Fe_3O_4NPs]-BPED-Cu(II) supported catalyst and various catalysts for the homocoupling of phenylacetylene is highlighted in **Table 5**.

Table 5. Comparison of the experimental results obtained for the homocoupling of phenylacetylene in presence of different catalysts.

Catalyst	Experimental conditions	Phenylacetylene (Initial weight content, mg	Cu(II) (weight content, mg)	Yields (%)	Regeneration number of cycles	Ref.
$Cu(OAC)_2$ (H_2O)	DMSO, 90 °C, air, 10h,	**102**	**63.5**	**90**	**-**	**[66]**
SBA-15-Cu(II)	DMSO, 100 °C, air, 4h	**102**	**2.8**	**97**	**-**	**[39]**
HMS-DP-Cu(II)	EtOH, 80 °C, air, 8h	**102**	**5.2**	**97**	**3**	**[57]**
Ps-TEDETA-$CuSO_4$	Piperidine, Toluene, 60°C, air, 24h	**102**	**3.2**	**96**	**9**	**[67]**
Cu/Cu_2ONPs@rGO	Cs_2CO_3, EtOH, 80 °C, O_2, 8h	**102**	**2.6**	**99**	**7**	**[68]**
[(GO-EDA-CAC)@Fe_3O_4NPs]-BPED-Cu(II)	Na_2CO_3, Glycerol, 80 °C, air, 120min.	**102**	**2.4**	**99**	**15**	**This work**

Narani *et al.,* [39] reported a Cu(II) complex heterogenized on (N1-propylethane1,2-diamine)triethoxysilane (Cu(II)-N,N-SBA-15) for the homocoupling reaction of phenylacetylene IN dmso and they obtained a yield of 97% in 4 hours at 100 °C which is slightly higher than the one obtained with the homogenous $Cu(OAC)_2(H_2O)$ catalyst [66]. This result may be explained by the use of a lower reaction temperature (90 °C). Nevertheless, these results are slightly lower than that of Cu/Cu2ONPs supported reduced graphene oxide sheets (Cu/Cu_2ONPs@rGO) [68] and it we can also be concluded that our

[GO-EDA-CAC)@Fe_3O_4NPs]-BPED-Cu(II) supported catalyst exhibits the higher catalytic activity for the homocoupling of phenylacetylene in comparison with the results reported in the literature because the reaction time (e.g. 120 min.) is much lower than other catalysts (a few hours). Moreover, it was regenerated several times, more than 15 cycles.

4. Conclusion

The results of the present investigation showed that the graphene oxide (GO) sheets was successfully modified with magnetite nanoparticles (Fe_3O_4NPs) through a co-precipitation method for high-efficiency removal of Cu(II) ions from aqueous solutions. The effects of pH and contact time on the adsorption of Cu(II) ions by the different adsorbents were systematically studied and it was demonstrated that the [(GO-EDA-CAC)@Fe_3O_4NPs]-BPED absorbent exhibited the highest Cu(II) ions adsorption capacity (e.g. 3.8 $mmol.g^{-1}$) at a pH of 7. Moroever, the pseudo-second-order model was the most appropriate one to describe the adsorption of Cu(II) ions from aqueous solutions. Then, the recovered [GO-EDA-CAC@Fe_3O_4NPs]-BPED-Cu(II) was recycled as an efficient supported catalyst for the homocoupling of terminal alkynes and it lead to the highest catalytic performance for the homocoupling of phenylacetylene with a yield up to 99%, under green conditions. Furthermore, the [GO-EDA-CAC@Fe_3O_4NPs]-BPED-Cu(II) supported catalyst has been reused for fifteen times without a significant loss of its activity, making it acceptable for industrial-scale production.

Declaration of interests

The authors declare that they have no known competing for financial interests or personal relationships that could have appeared to influence the work reported in this paper.

Acknowledgments

The authors gratefully acknowledge the financial support from the Tunisian Ministry of High Education and Scientific Research, Institut Français de Tunisie (Ambassade de France en Tunisie) and all the staff of the technological center of microstructures of the University of Lyon 1 for their technical help. We would to thank Mrs. BRUNON Céline for her help in the XPS analysis.

References

[1] T. Boningari, D.K. Pappas, P.G. Smirniotis, Metal oxide-confined interweaved titania nanotubes M/TNT (M = Mn, Cu, Ce, Fe, V, Cr, and Co) for the selective catalytic reduction of NOx in the presence of excess oxygen, J. Catal. 365 (2018) 320-333.

[2] F. Liu, H. He, Z. Lian, W. Shan, L. Xie, K. Asakura, W. Yang, H. Deng, Highly dispersed iron vanadate catalyst supported on TiO2 for the selective catalytic reduction of NOx with NH3, J. Catal. 307 (2013) 340-35.

[3] J. Z. Y. Tan, N N. M. ursam, F. Xia, M. A. Sani, W. Li,; X. D. Wang, R. A. Caruso, High-Performance Coral Reef-like Carbon Nitrides: Synthesis and Application in Photocatalysis and Heavy Metal Ion Adsorption, ACS Appl. Mater. Interfaces. 9 (2017) 4540-4547.

[4] I. Uoginte, G. Lujaniene, K. Mazeika, Study of Cu (II), Co (II), Ni (II) and Pb (II) removal from aqueous solutions using magnetic Prussian blue nano-sorbent. J. Hazard. Mater. 369 (2019) 226-235.

[5] L. Chaabane, H. chahdoura, W. Moslah, M. Snoussi, E. Beyou, M. Lahcini, N.S. Abid, M.H.V. Baouab, Synthesis and characterization of Ni (II), Cu (II), Fe (II) and Fe3O4 nanoparticle complexes with tetraaza macrocyclic Schiff base ligand for antimicrobial activity and cytotoxic activity against cancer and normal cells, Appl Organometal. Chem., 5 (2019) 1-19.

[6] T. Jiang, W. Liu, Y. Mao, L. Zhang, J. Cheng, M. Gong, H. Zhao, L. Dai, S. Zhang, Q. Zhao, Adsorption behavior of copper ions from aqueous solution onto graphene oxide–CdS composite. Chem. Eng. J. 259 (2015) 603-610.

[7] Y. Chen, M. He, C. Wang, Y. Wie, A novel polyvinyltetrazole-grafted resin with high capacity for adsorption of Pb(II), Cu(II) and Cr(III) ions from aqueous solutions J. Mater. Chem. A. 2 (2014) 10444-10453.

[8] M.A. Barakat, New trends in removing heavy metals from industrial wastewater. Arab. J. Chem. 4 (2011) 361-377.

[9] I. Duru, D. Ege, A.R. Kamali, Graphene oxides for removal of heavy and precious metals from wastewater. J. Mater. Sci. 51 (2016) 6097-6116.

[10] B. Xiang, D. Ling, H. Lou, H. Gu, 3D hierarchical flower-like nickel ferrite/manganese dioxide toward lead (II) removal from aqueous water. J. Hazard. Mater. 325 (2017) 178-188.

[11] S. Yuan, J. Gu, Y. Zheng, W. Jiang, B. Liang, S. O. Pehkonen, Purification of phenol-contaminated water by adsorption with quaternized poly(dimethylaminopropyl methacrylamide)-grafted PVBC microspheres. J. Mater. Chem. A. 3 (2015) 4620-4636.

[12] R. Kumara, R.K. Sharmac, A. P. Singh, Sorption of Ni(II), Pb(II) and Cu(II) ions from aqueous solutions by cellulose grafted with poly(HEMA-co-AAc): Kinetic, isotherm and thermodynamic study J. Environ. Chem. Eng., 4 (2019) 103088.

[13] G. Zhao, X. Huang, Z. Tang, Q. Huang, F. Niu, X. Wang. Polymer-based nanocomposites for heavy metal ions removal from aqueous solution: a review Polym. Chem. 9 (2018) 3562-3582.

[14] C. J. Madadrang, H. Y. Kim, G. Gao, N. Wang, J. Zhu, H. Feng, M. Gorring, M. L. Kasner, S. Hou, Adsorption Behavior of EDTA-Graphene Oxide for Pb (II) Removal. ACS Appl. Mater. Interfaces, 4 (2012) 1186-1193.

[15] J. C. Moreno, R. Gómez, L. Giraldo, Removal of Mn, Fe, Ni and Cu Ions from Wastewater Using Cow Bone Charcoal. Materials, 3 (2010) 452-466.

[16] B. I. Olu-Owolabi, A. H. Alabi, E.I. Unuabonah, P.N. Diagboya, L. Böhm, R.A. Düring, Calcined biomass-modified bentonite clay for removal of aqueous metal ions. J. Environ. Chem. Eng. 4 (2016) 1376-1382.

[17] F.A. I. Al-Khaldi, B. Abu-Sharkh, A.M. Abulkibash, M.I. Qureshi, T. Laoui, M.A. Atieh, Effect of acid modification on adsorption of hexavalent chromium (Cr(VI)) from aqueous solution by activated carbon and carbon nanotubes. Desalin. Water Treat. 837 (2015) 1-13.

[18] J. Wang, Z. Li, S. Li, W. Qi, P. Liu, F. Liu, Y. Ye, L. Wu, L.Wang, W. Wu, Adsorption of Cu (II) on oxidized multi-walled carbon nanotubes in the presence of hydroxylated and carboxylated fullerenes, Plos one, 8 (2013) e72475.

[19] R. Sitko, P. Janik, B. Fiest, E. Talik, A. Gagor, Suspended Aminosilanized Graphene Oxide Nanosheets for Selective Preconcentration of Lead Ions and Ultrasensitive Determination by Electrothermal Atomic Absorption Spectrometry. ACS Appl. Mater. Interfaces, 22 (2014) 20144-20153.

[20] A. Guimont, E. Beyou, P. Cassagnau, G. Martin, P. Sonntag, F. D'Agosto, C. Boisson. Grafting of polyethylene onto graphite oxide sheets: a comparison of two routes Polym. Chem. 4 (2013) 2828-2836.

[21] A. Pazat, E. Beyou, C. Barres, F. Bruno, C. Janin, In situ emulsion cationic polymerization of isoprene onto the surface of graphite oxide sheets. Appl. Surf, Sci, 396 (2017) 902-911.

[22] S. T. Yang, Y. L. Chang, H. F. Wang, G. B. Liu, S. Chen, Y. W. Wang, Y. F. Liu and A. N. Cao. Folding/aggregation of graphene oxide and its application in Cu^{2+} removal. J. Colloid Interface Sci., 351 (2010) 122–127.

[23] K. Gul, S. Sohni, M. Waqar, F. Ahmad, N.A.N. Norulaini, A.K.O. Mohd. Functionalization of magnetic chitosan with graphene oxide for removal of cationic and anionic dyes from aqueous solution. Carbohydr. Polym. 152 (2016) 520-531.

[24] D. Chen, H. Zhang, K. Yang, H. Wang, Functionalization of 4-aminothiophenol and 3-aminopropyltriethoxysilane with graphene oxide for potential dye and copper removal J. Hazard. Mater. 310 (2016) 179-187.

[25] L. Chaabane, E. Beyou, A. El Ghali, M. H. V. Baouab, Comparative studies on the adsorption of metal ions from aqueous solutions using various functionalized graphene oxide sheets as supported adsorbents, J. Hazard. Mater. doi.org/10.1016/j.jhazmat.2019.121839.

[26] D. Zhao, X. Gao, C. Wu, R. Xie, S. Feng, C. Chen,. Facile preparation of amino functionalized graphene oxide decorated with Fe_3O_4 nanoparticles for the adsorption of Cr(VI). Appl. Surf. Sci., 384 (2016) 1–9.

[27] S. Tong, C. A. Quinto, L. Zhang, P. Mohindra, G. Bao, Size-Dependent Heating of Magnetic Iron Oxide Nanoparticles, ACS Nano. 11 (2017) 6808-6816.

[28] Y. Yoon, W.K. Park, T.M. Hwang, D.H. Yoon, W.S. Yang, J.W. Kang, Comparative evaluation of magnetite-graphene oxide and magnetite-reduced graphene oxide composite for As(III) and As(V) removal. J. Hazard. Mater. 304 (2016)196-204.

[29] W. Wu, Z.Wu, T. Yu, C. Jiang, W. S. Kim, Recent progress on magnetic iron oxide nanoparticles: synthesis, surface functional strategies and biomedical applications, Sci. Technol. Adv. Mater. 16 (2015) 023501.

[30] R. Mehdaoui, L, Chaabane, E. Beyou, M.H.V. Baouab, Sono-heterogeneous Fenton system for degradation of AB74 dye over a new tetraaza macrocyclic Schiff base cellulose ligand-loaded Fe_3O_4 nanoparticles J. Iran. Chem. Soc., 16 (2019) 645–659.

[31] S. Liu, H. Wang, L. Chai, M. Li, Effects of single- and multi-organic acid ligands on adsorption of copper by Fe_3O_4/graphene oxide-supported DCTA. J. Colloid Interface Sci. 478 (2016) 288–295.

[32] L. Su, J. Dong, L. Liu, M. Sun, R. Qiu, Y. Zhou, S. Yin, Copper catalysis for selective heterocoupling of terminal alkynes, J. Am. Chem. Soc. 138 (2016) 12348–12351.

[33] K. S. Sindhu, G. Anilkumar, Recent advances and applications of Glaser coupling employing greener protocols, RSC Adv. 4 (2014) 27867–27887.

[34] D. Wang, J. Li, N. Li, T. Gao, S. Houa, B. Chen, An efficient approach to homocoupling of terminal alkynes: Solvent-free synthesis of 1,3-diynes using catalytic Cu(ii) and base. Green Chem. 12 (2010) 45-48.

[35] M. Singh, A. S. Singh, N. Mishra, A. K. Agrahari, V. K. Tiwari, Benzotriazole as an efficient ligand in Cu-Catalyzed glaser reaction, ACS Omega 4, (2019) 2418-2424.

[36] B. Vilhanová, J. Václavík, L. Artiglia, M. Ranocchiari, A. Togni, J.A.V. Bokhoven, Subnanometer gold clusters on amino-functionalized silica: an efficient catalyst for the synthesis of 1,3-diynes by oxidative alkyne coupling, ACS Catal. 7 (2017) 3414-3418.

[37] R. Xiao, R. Yao, M. Cai, Practical Oxidative homo-and heterocoupling of terminal alkynes catalyzed by immobilized copper in MCM-41, Eur. J. Org. Chem., 5 (2012) 4178-4184.

[38] P. Kuhn, A. Alix, M. Kumarraja, B. Louis, P. Pale, J. Sommer, Copper–zeolites as catalysts for the coupling of terminal alkynes: an efficient synthesis of diynes, Eur. J. Org. Chem., 3 (2009) 423-429.

[39] A. Narani, R. K. Marella, P. Ramudu, K. S. R. Rao, D. R. Burri, Cu(II) complex heterogenized on SBA-15: a highly efficient and additive-free solid catalyst for the homocoupling of alkynes, RSC Adv., 4 (2014) 3774-3781.

[40] P.M. Chauhan, S.N. Thummar, K.H. Chikhalia, Design, Synthesis, bioactivity, and computational studies of some morpholine-clubbed coumarinyl acetamide and cinnamide derivaties, J. Iran, Chem. Sco. 15 (2018) 1261–1277.

[41] A. El Ghali, M.H.V. Baouab, M.S. Roudesli. Aminated cotton fibers loaded with copper(II) ions for enhanced pesticide removal performance from water in a laboratory scale batch. Ind. Crops Prod. 39 (2012) 139-148.

[42] F. Samadaei, M.S. Kalajahi, H.R. Mamaqani, M. Banaei, A structural study on ethylenediamine-and poly(amidoamine)-functionalized graphene oxide: simultaneous reduction, functionalization, and formation of 3D structure. RSC.Adv. 5 (2015) 71835-71843.

[43] M. A. Akhtar, R. Batool, A. Hayat, D. Han, S. Riaz, S.U. Khan, M. Nasir, M.H. Nawaz , L. Niu, Functionalized Graphene Oxide Bridging between Enzyme and Au-Sputtered Screen-Printed Interface for Glucose Detection. ACS Appl. Nano Mater., 2 (2019)1589-1596.

[44] W. S. Mohamed, A. M. Abu-Dief, Synthesis, characterization and photocatalysis enhancement of Eu2O3-ZnO mixed oxide nanoparticles, J. Phys. Chem. Solid, 116 (2018) 375-385.

[45] J.S. Lee, C.J. Myung, H.Y. Yoon, J.K. Lee, Y.K. Kim, Magnetic multi-granule nanoclusters: A model system that exhibits universal size effect of magnetic coercivity, Sci. Rep. 5 (2015) 12135.

[46] E. E. Carpenter, Iron nanoparticles as potential magnetic carriers, J. Magn. Magn. Mater. 225 (2001) 17-20.

[47] M. Mikhaylova, D. K. Kim, N. Bobrysheva, M. Osmolowsky, V. Semenov, T. Tsakalakos, M. Muhammed, Langmuir 20 (2004) 2472-2477.

[48] P. H. Linh, N. V. Chien, D. D. Dung, P. H. Nam, D. T. Hoa, N. T. N. Anh, L. V. Hong, N. X. Phuc, P. T. Phong, Biocompatible nanoclusters of O-carboxymethyl chitosan-coated Fe3O4 nanoparticles: synthesis, characterization and magnetic heating efficiency, J. Mater. Sci. 53 (2018) 8887-8900.

[49] H. T. Xing, J. H. Chen, X. Sun, Y. H. Huang, Z. B. Su, S. R. Hu, W. Weng, S. X. Li, H. X. Guo, W. B. Wu, Y. S. He, F. M. Li, Y. Huang, NH_2-rich polymer/graphene oxide use as a

novel adsorbent for removal of Cu(II) from aqueous solution, Chem. Eng. J. 263 (2015) 280-289.

[50] X. Wang, S. Jing, Y. Liu, X. Qiua, Y. Tan, Preparation of dithiocarbamate polymer brush grafted nanocomposites for rapid and enhanced capture of heavy metal ions, RSC Advances, 7 (2017) 13112-13122.

[51] C. R. Lee, H. S. Kim, I. H. Jang, J. H. Im, N.G Park, Pseudo First-Order Adsorption Kinetics of N719 Dye on TiO2 Surface, ACS Appl. Mater. Interfaces, 36 (2011) 1953-1957.

[52] Y. Xiao, J. Azaiez, J.M. Hill, Erroneous Application of Pseudo-Second-Order Adsorption Kinetics Model: Ignored Assumptions and Spurious Correlations, Ind. Eng. Chem. Res. 577 (2018) 2705-2709.

[53] R. S. Juang, M. L. Chen, Application of the Elovich Equation to the Kinetics of Metal Sorption with Solvent-Impregnated Resins, Ind. Eng. Chem. Res., 36 (1997) 813-820.

[54] Z. Abdeen, S.G. Mohammad, M.S. Mahmoud, Adsorption of Mn (II) ion on polyvinyl alcohol/chitosan dry blending from aqueous solution, Environ. Nanotechnol. Monit, Manage. 3 (2015) 1-9.

[55] B. Nayak, A. Samant, R. Patel, P. K. Misra,Comprehensive Understanding of the Kinetics and Mechanism of Fluoride Removal over a Potent Nanocrystalline Hydroxyapatite Surface, ACS Omega, 211 (2017) 8118-8128.

[56] H. Medhi, K. G. Bhattacharyya, Kinetic and mechanistic studies on adsorption of Cu(ii) in aqueous medium onto montmorillonite K10 and its modified derivative, New J. Chem., 41 (2017) 13533-13552.

[57] F. Alons, M. Yus, Heterogeneous Catalytic Homocoupling of Terminal Alkynes, ACS Catal. 2 (2012) 1441-1451.

[58] A. Sagadevan, P. C. Lyub, K. C. Hwang, Visible-light-activated copper(i) catalyzed oxidative Csp–Csp cross-coupling reaction: efficient synthesis of unsymmetrical conjugated diynes without ligands and base, Green Chem., 18 (2016) 4526-4530.

[59] A. Sagadevan, A. Ragupathi, C. C. Lin, J. R. Hwu and K. C. Hwang, Visible-Light Initiated Copper(I)-Catalysed Oxidative C-N Coupling of Anilines with Terminal Alkynes: OneStep Synthesis of α-Ketoamides, Green Chem. 17 (2015) 1113-1119.

[60] R. A. Sheldon, Metrics of Green Chemistry and Sustainability: Past, Present, and Future, ACS Sustainable Chem. Eng. 6, (2018) 32-48.

[61] R. T. A. Tirumalaa, A. P. Dadgara, F. Mohammadparasta, S. B. Ramakrishnana, T. Moub, B. Wangb, M. Andiappana, Homogeneous versus Heterogeneous Catalysis in Cu2Onanoparticle-catalyzed C-C Coupling Reactions, Green Chem. 21 (2019) 5284-5290.

[62] A. E. King, L. M. Huffman, A. Casitas, M. Costas, X. Ribas, S. S. Stahl, Copper-Catalyzed Aerobic Oxidative Functionalization of an Arene C−H Bond: Evidence for an Aryl-Copper(III) Intermediate, J. Am. Chem. Soc., 132 (2010) 12068-12073.

[63] M. H. Vilhelmsen, J. Jensen, C. G. Tortzen, M. B. Nielsen, The Glaser–Hay Reaction: Optimization and Scope Based on 13C NMR Kinetics Experiments, Eur. J. Org. Chem., 4 (2013) 701-711.

[64] G. Zhang, H. Yi, G. Zhang, Y. Deng, R. Bai, H. Zhang, J. T. Miller, A. J. Kropf, E. E. Bunel, A. Lei, Direct observation of reduction of Cu (II) to Cu (I) by terminal alkynes, J. Am. Chem. Soc., 3 (2014) 924-926.

[65] N. Devarajan, M. Karthika, P. Suresh, Copper catalyzed oxidative homocoupling of terminal alkynes to 1,3-diynes: a Cu3(BTC)2 MOF as an efficient and ligand free catalyst for Glaser–Hay coupling, Org. Biomol. Chem., 15 (2017) 9191-9199.

[66] X. Jia, K. Yin, C. Li, J. Lia, H. Biana, Copper-catalyzed oxidative alkyne homocoupling without palladium, ligands and base, Green Chem., 13 (2011) 2175-2178.

[67] S. Yan, S. Pan, T. Osako, Y. Uozumi, Recyclable Polystyrene-Supported Copper Catalysts for the Aerobic Oxidative Homocoupling of Terminal Alkynes, Synlett, 27 (2016) 1232-1236.

[68] W. Lu, W. Sun, X. Tan, L. Gao, G. Zheng, Stabilized Cu/Cu2O nanoparticles on rGO as an efficient heterogeneous catalyst for Glaser homo-coupling, Catal. Commun. 125 (2019) 98-102.

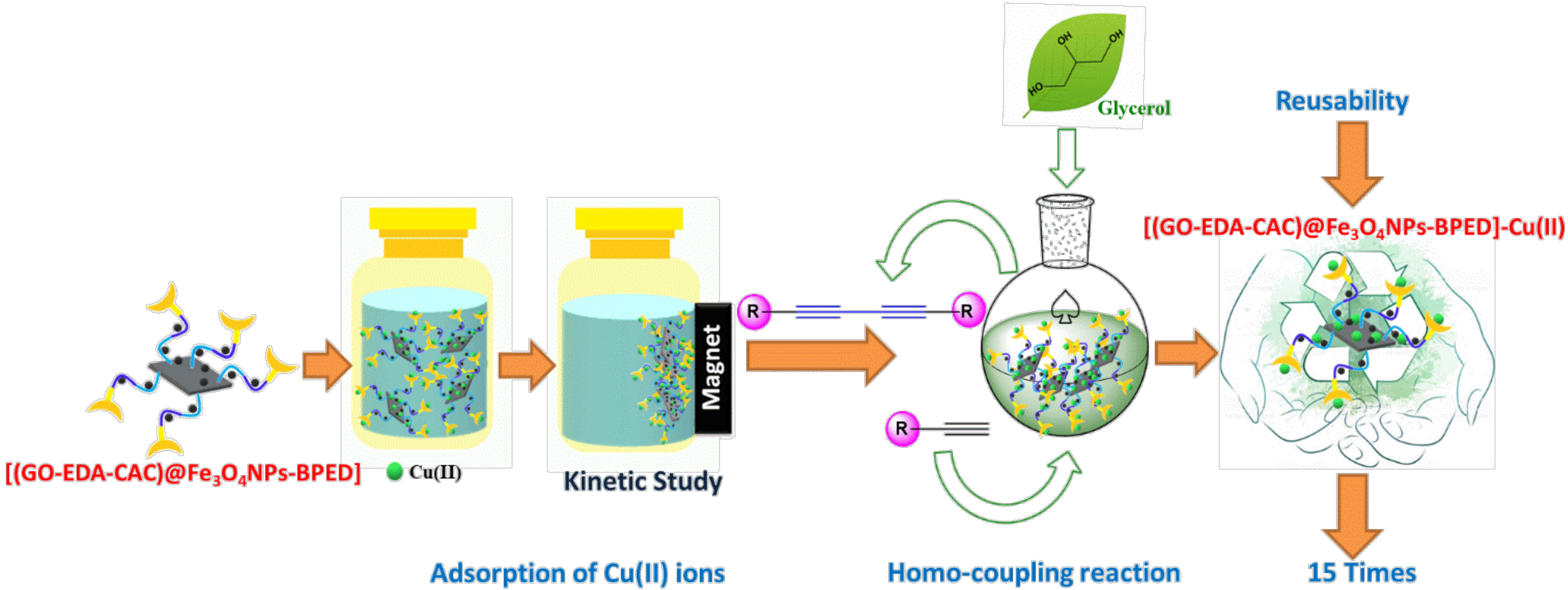
Glycerol
OH
OH
HO
Reusability
[(GO-EDA-CAC)@Fe3O4NPs-BPED]-Cu(II)
[(GO-EDA-CAC)@Fe3O4NPs-BPED]
Cu(II)
Magnet
Kinetic Study
R
R
R
Adsorption of Cu(II) ions
Homo-coupling reaction
15 Times